RSC Advances

Enhancing Photovoltaics with Broadband High-Transparency Glass Using Porosity-Tuned Multilayer Silica Nanoparticle Anti-Reflective Coatings

Journal:	*RSC Advances*
Manuscript ID:	RA-ART-04-2014-003465.R1
Article Type:	Paper
Date Submitted by the Author:	13-Jun-2014

Complete List of Authors:	Loh, Joel; University of Toronto, Electrical and Computer Engineering Puzzo, Daniel; University of Toronto, Chemistry O'brien, Paul; University of Toronto, Materials Science and Engineering Ozin, Geoffrey; University of Toronto, Chemistry Kherani, Nazir; University of Toronto, Canada, Department of Electrical and Computer Engineering, and Department of Materials Science and Engineering

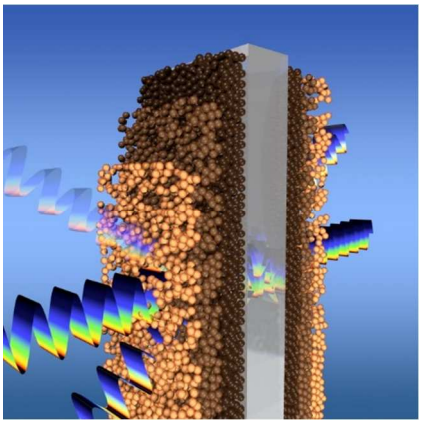

The performance of optoelectronic devices using glass envelopes can be improved substantially by the application of an effective anti-reflective coating. In this paper, we investigate the preparation of low index films through modulation of the porosity of silica nanoparticle films. Porosity variation is accomplished by introducing polystyrene porogen within colloidal silica nanoparticle films, which are deposited in a controlled manner, followed by pyrolysis of the porogen. Multilayer stacks of nanoparticle films with varying degrees of porosity were fabricated by sequentially spin coating and sintering various silica/polystyrene mixtures. The average transmittance (400-1000 nm) of Corning glass was improved from 91.0% to 95.2% using a three layer stack on one glass-air interface, and to 99.0% using three layer stacks on both interfaces – the highest reported values for facile synthesized multilayer structures. Utilization of the single and dual interface high transparency glass placed on a crystalline silicon solar cell leads to increased photocurrent densities by 4.0% and 6.0% absolute, respectively, relative to uncoated glass.

Enhancing Photovoltaics with Broadband High-Transparency Glass Using Porosity-Tuned Multilayer Silica Nanoparticle Anti-Reflective Coatings

Joel Y.Y. Loh[†], Daniel P. Puzzo[†,‡], Paul G. O'Brien[‡,§], Geoffrey A. Ozin[§], Nazir P. Kherani[†,‡,*]

[†]Department of Electrical and Computing Engineering, University of Toronto, 10 King's College Road, Toronto, Ontario, Canada M5S 3G4

[‡]Department of Materials Science and Engineering, University of Toronto, 184 College Street, Toronto, Ontario, Canada M5S 3E4

[§]Department of Chemistry, University of Toronto, 80 St. George Street, Toronto, Ontario, Canada, M5S 3H6

*kherani@ecf.utoronto.ca

Keywords: Anti-reflective coatings, porous nanoparticle films, high transparency glass, silicon nanoparticles, polystyrene porogens, silicon solar cell

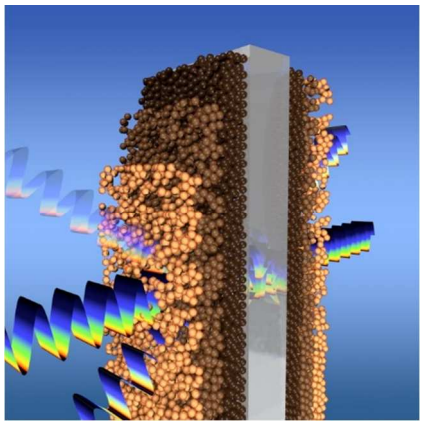

ABSTRACT: The performance of optoelectronic devices using glass envelopes can be improved substantially by the application of an effective anti-reflective coating. In this paper, we investigate the preparation of low index films through modulation of the porosity of silica nanoparticle films. Porosity variation is accomplished by introducing polystyrene porogen within colloidal silica nanoparticle films, which are deposited in a controlled manner, followed by pyrolysis of the porogen. Multilayer stacks of nanoparticle films with varying degrees of porosity were fabricated by sequentially spin coating and sintering various silica/polystyrene mixtures. The average transmittance (400-1000 nm) of Corning glass was improved from 91.0% to 95.2% using a three layer stack on one glass-air interface, and to 99.0% using three layer stacks on both interfaces – the highest reported values for facile synthesized multilayer structures. Utilization of the single and dual interface high

transparency glass placed on a crystalline silicon solar cell leads to increased photocurrent densities by 4.0% and 6.0% absolute, respectively, relative to uncoated glass.

Introduction

The design and ease of fabrication of broadband and directionally invariant anti-reflective coatings[1,2] (ARCs) is limited by the available fixed refractive index antireflective (AR) materials; common low to medium index materials include MgF_2, Si_3N_4 and TiO_2 with indices of 1.38, 1.95 and 2.35, respectively. Hence, ARC designs range from the single quarter wavelength layer minimizing transmittance at a single wavelength value, quarter-half wavelength two layer ARC minimizing reflectance at two wavelength values while simultaneously broadening transmittance, to elaborate multi-layer systems of more than a dozen layers to achieve minimal reflectance over a large wavelength range. The integration of designer-specified indices into a multi-layered ARC that can be readily and economically fabricated to attain highly transparent glass would aid immensely in enhancing light transmission and hence the performance of optical devices. Moreover, enhanced utilization of the solar spectrum with the transition from single to tandem to multijunction solar cells further intensifies the need for broadband ARCs due to increased interfaces[3,4]. Thus, complete broad-band and directionally-invariant coupling of solar light into the encapsulating glass and the underlying solar cell will result in marked gains in photogenerated power of up to 10% in the visible. The fabrication of antireflective coatings has employed both top-down and bottom-up techniques.[5-7] A stack of 75 layers comprising 4 different materials on a glass surface can produce an average broad-band reflectivity of less than 0.2%[8]; while this result is impressive, such a physical vapor

deposition technique is deemed both onerous and economically impractical for large area applications. Recently, application of the GLancing Angle Deposition (GLAD) technique[9] reported a two-layered ARC on both glass surfaces yielding an average transmissivity[10] of 98.2% over a 400 nm to 1000 nm wavelength range; a striking result but also considered to be unfeasible for large area production. In a manner similar to the GLAD technique of introducing porosity to control refractive index, mesoporous silica nanoparticles dispersed in methanol mixed with a variable amount of tetraethyl orthosilicate (TEOS) binder yielded a porous single layer ARC of index 1.27 with a high transmittance at a single wavelength[11]. Inducing porosity in silica films can be also initiated by plasma roughening of an acrylate layer on a PET substrate, followed by chemical vapor deposition of silica nanoparticles[12]. In both instances, however, lower index films or graded index configurations have not been reported - criteria required to achieve a truly broadband ARC. Solution phase methods offer a potentially viable and economical avenue of creating controlled index graded layers.[13-15] Within this framework, sol-gel techniques have been studied extensively and have resulted in demonstrated transmissivities of 99.4 % to 99.8 % over a narrow band of 450 nm to 700 nm on a glass substrate.[14] However, owing to the sensitivity of the reaction kinetics of the process and the accompanying limitation in the lowest index achievable, truly broad-band sol-gel ARCs remain an active area of research[15]. In contrast to the above described homogeneous ARCs, significant strides have been made in the development of inhomogeneous ARCs using textured periodic and aperiodic nanostructures.[18-25] Using e-beam lithography on PMMA resin which was deposited on both glass surfaces,[24] hyperbolic subwavelength structures exhibit average transmittance of

99.58% over the visible. Inhomogeneous thin film structures provide an ideal platform for ARCs but are difficult and costly to implement on a large scale due to the need for precise variation of material tapering and packing on the nanometer scale, despite the advent of embossing methods that produce patterned templates.[27,28] To that end, the exploration of simpler geometries such as hexagonal lattices of polystyrene cylindrical nanopillars on quartz substrates has resulted in achieving high transmittances at large incident angles.[29]

In this paper, we explore facile fabrication of ARCs comprising tunable refractive indices via controlled introduction of porosity in silica nanoparticle films. The porosity is enabled by the introduction of polystyrene nanoparticles within the silica nanoparticle colloidal solution, followed by pyrolysis of the polystyrene from within the silica nanoparticle matrix after spin coating onto a substrate. Using this approach we modulate the void fraction and refractive index of the silica nanoparticle films, enabling realization of low index layers. Guided by genetic algorithm[30–32] and Abeles' matrix optimization, multi-layered index-graded nanoparticle films were deposited on single and dual glass surfaces to exhibit broadband high transparency glass in the visible. Herein we report the highest average transmittance over a 600 nm broadband wavelength range using a facile synthesized multilayer structure amenable for photovoltaics and allied applications. We also demonstrate the integration of our structures in silicon photovoltaics and show a 6% enhancement in light capture which is equivalent to a power increase of 6 GWp (gigawatts peak) based on 100 GWp of cumulative global PV installed currently.

ARC Fabrication

We systematically synthesize a range of porosity-varying silica nanoparticle films and characterize their porosities and refractive indices; we denote these as single layer films. Subsequently, specific index-varying nanoparticle films are integrated into a multilayer stack to render the desired ARC. The single-layer porous films are fabricated on a polished (100) crystalline silicon substrate by spin coating a colloidal mixture of silica and polystyrene nanoparticles followed by a sintering process. The colloidal mixture consists of 10nm (±2nm) diameter silicon dioxide (SiO_2) nanoparticles (30%wt/v, 1.27×10^{15} particles/mg) in aqueous suspension (Ludox 420794) and 50nm (±7.5nm) diameter polystyrene (PS) nanoparticles (2.5%w/v, 1.456×10^{13} particles/mg) in aqueous suspension (Polybead© microspheres, Polyscience Inc. 08691-10) (Figure. 3-2). First, one part of the SiO_2 solution is diluted with *n* parts of deionized (DI) water to obtain a 1:*n* dilution, where *n* varies from 0 to 7. Next, 15mg of the diluted SiO_2 solution is mixed with varying amounts of the PS colloidal solution. The SiO_2/PS mixture is diluted with 100mg of DI water to obtain the working colloidal mixture. This SiO_2/PS mixture is then spin coated onto silicon substrates at 3500RPM for 1 minute using an acceleration rate of 200RPM/sec^2. The resultant film is then sintered in ambient atmosphere at 450°C for 1 hour with a ramp rate of 40°C/min. The refractive indices at 633nm and thickness of the single layer porous silica nanoparticle films are determined by spectral ellipsometry (SE) (Sopra GES5-E). An estimate of the variance in the index and thickness of the films was measured on 2 spots on three films made with identical solutions. Porosity volume fractions and pore size distributions were determined using the atmospheric ellipso-porosimetry technique[33] for selected films.

The synthesis of a discrete multilayer stack ARC involved consecutive layering of appropriate single-layer films. To prevent intermixing of the individual layers, we introduced a layer of 20nm (±2nm) diameter PS (1%w/v colloidal solution, Applied Physics, Inc. 3020A) between the single-porous layers. Specifically, we spin-coat all the single-layer SiO_2/PS films and the intermediate PS layers consecutively (Figure 1) and then sinter the entire stack. The use of 50nm diameter PS intermediate layers yielded films of poor morphology.

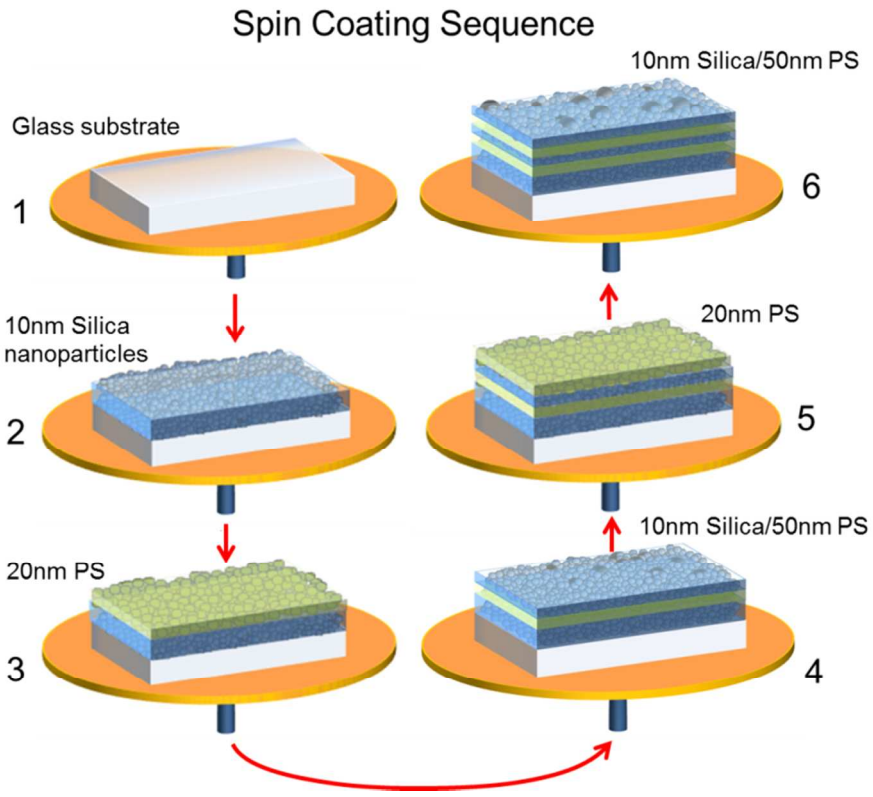

Figure 1. An illustration of the spin-coating sequence for a multilayer ARC. 1) cleaned glass substrate; 2) polystyrene-free silica solution on glass; 3) 20nm diameter PS solution on the silica layer; 4) SiO_2/PS mixture on the 20nm PS intermediate layer; 5) 20nm PS solution on the first SiO_2/PS layer; and 6) second SiO_2/PS mixture on the 20nm PS layer. Illustration is not to scale.

Results and discussion

The refractive indices and physical thicknesses of the single layer silica films measured as a function of PS:SiO_2 solution mass ratios are shown in Figures 2a and 2b, respectively. The pore size distribution of silica films (prepared from pre-diluted silica of 1:1) as a function of PS:SiO_2 solution mass ratios is shown in Figure 2c and the porosity of selected films is shown as the inset in Figure 2c. Topographical and cross sectional SEM images of several single-layer silica films are shown in Figure 3. The film thicknesses as obtained from the SEM images were observed to be within 10nm of the SE derived thicknesses. The refractive indices of the SiO_2 films (for all pre-dilutions) synthesized without the use of PS ranges from 1.27 to 1.34 while the porosity is 33±3% with an average pore diameter of 3nm; a refractive index of 1.48±0.02 is inferred for a non-porous film. The SEM images (Figure 3) clearly indicate that PS-free SiO_2 films are compactly packed agglomerates of nanoparticles (Figure 3-a) and that the PS-based SiO_2 films become increasingly loose aggregates of nanoparticles with increasing PS to silica mass ratio (Figure 3-b to 3-d). For PS:SiO_2 mass ratio of ≤ 1:1, the porous films have well-defined circular pores embedded or extending through the film (Figure 3-b). For moderate PS:SiO_2 mass ratio of ≤ 5:1, the surface consists of circular mesopores and irregularly slit-shaped pores. This is also evident from the pore size distribution (Figure 2d) which displays a band of peaks in the 10-30nm radii range, and a long tail for pore radii ranging from 30 to 50nm. During the pyrolysis of the polystyrene particles it is conceivable that gaseous product is entrained in the capillary flow of the receding aqueous solvent which increases the capillary forces and thus draw the silica nanoparticles closer which in turn lead to the resulting slit-like pores. For large

PS:SiO_2 mass ratio of >~4.50, the films become much looser aggregates of individual particles with significantly less contact with neighboring particles (Figure 3-d(i -ii). For pre-dilutions of SiO_2 solution of greater than 3:1, the depth continuity is disrupted. The films now comprise an underlying porous layer of nanoparticles with clusters of nanoparticles situated thereupon (Figure 3-d-iii inset). The film ultimately becomes a disconnected accumulation of clusters (30-50 nm) of nanoparticles. The refractive index trend, exhibited in Figure 2a is observed to follow the overall porosity trend of Figure 2c inset. A linear and steep decrease in index from 1.34 to 1.20 is achieved for PS: SiO_2 ratio of < 1:1, while for PS: SiO_2 ratio of > 1:1 the index decreases more gradually from 1.20 to 1.10; this gradual decrease is attributed to the densification of the films. For even larger PS:SiO_2 ratios, the refractive index ranges between 1.07 and 1.11. With a high pre-diluted SiO_2 (>1:5) solution, a low refractive index can be achieved with PS:SiO_2 ratio of >4.0. In some samples with high SiO_2 dilution and high PS:SiO_2 ratios, the index is greater than 1.12 which indicates that the macro-porous network has undergone marked densification.

With increasing pre-dilution of the silica solutions the film thickness decreases from 330nm (1:0 dilution) to 80nm (1:7 dilution), due to a lower concentration of silica particles in the spin coated layer. For large amounts of PS mixed with highly pre-diluted SiO_2 solutions, the derived thicknesses are less than 50nm, which corresponds to the size of a PS nanoparticle; the films then resemble a discontinuous distribution of clusters of silica nanoparticles – in short a rough surface.

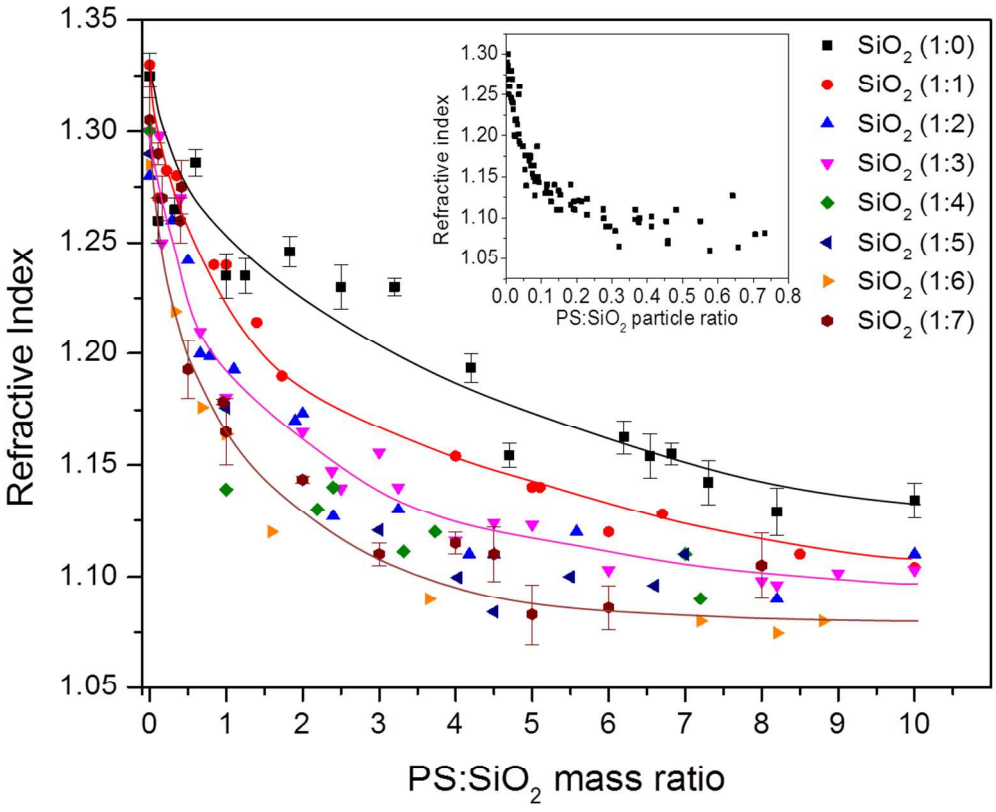

Figure 2. (a) Refractive indices of single-layer silica films as a function of the $PS:SiO_2$ solution mass ratio for a range of pre-dilutions (SiO_2:DI water = 1:0 to 1:7). The solid lines are visual guides. Inset: The refractive indices as a function of the estimated $PS:SiO_2$ particle ratio.

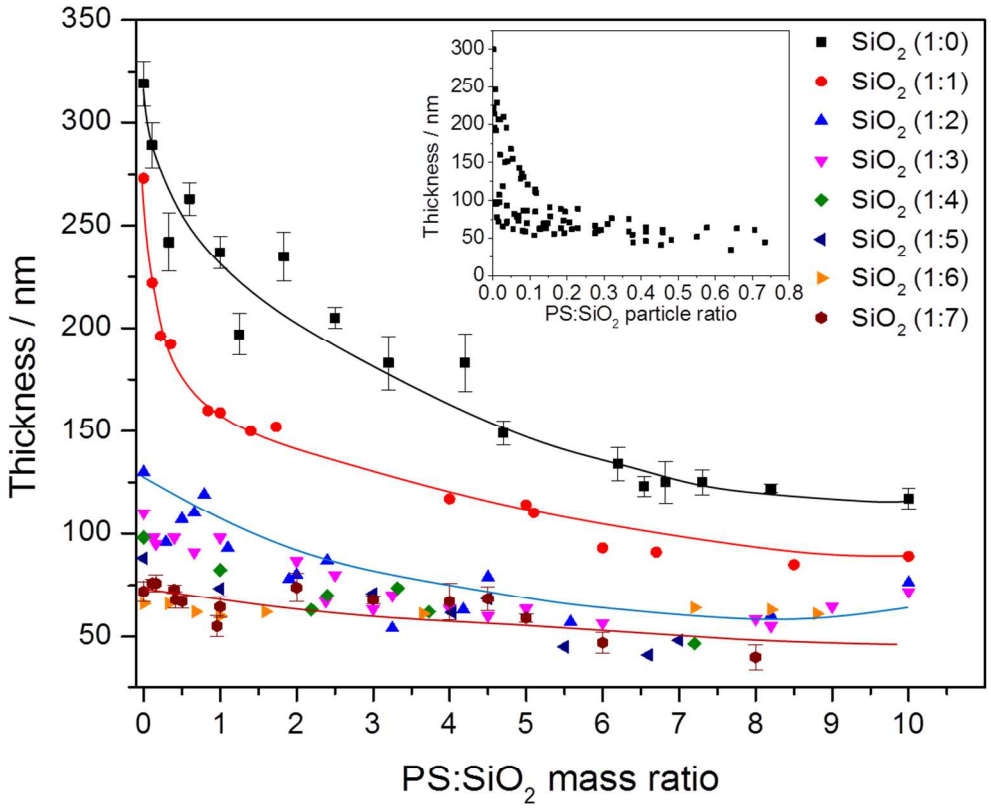

Figure 2. (b) Physical thicknesses of single-layer silica films as a function of the PS:SiO_2 solution mass ratio for a range of pre-dilutions (SiO_2:DI water = 1:0 to 1:7). The solid lines are visual guides. Film thicknesses were determined by spectroscopic ellipsometry. Inset: The thickness as a function of the estimated PS:SiO_2 particle ratio.

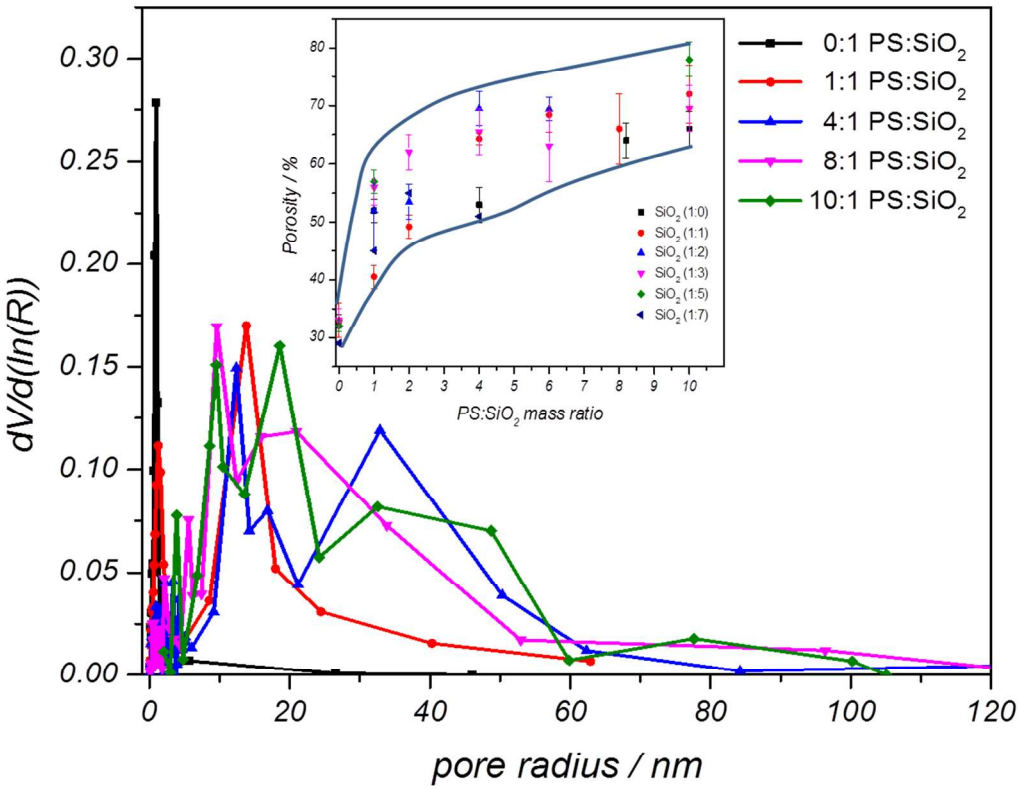

Figure 2. (c) Pore size distributions in silica nanoparticle films with increasing $PS:SiO_2$ solution mass ratios. The pre-dilution of the silica solution is 1:1 for the all the films. Inset: Porosity of nanoparticle films as a function of the $PS:SiO_2$ solution mass ratio.

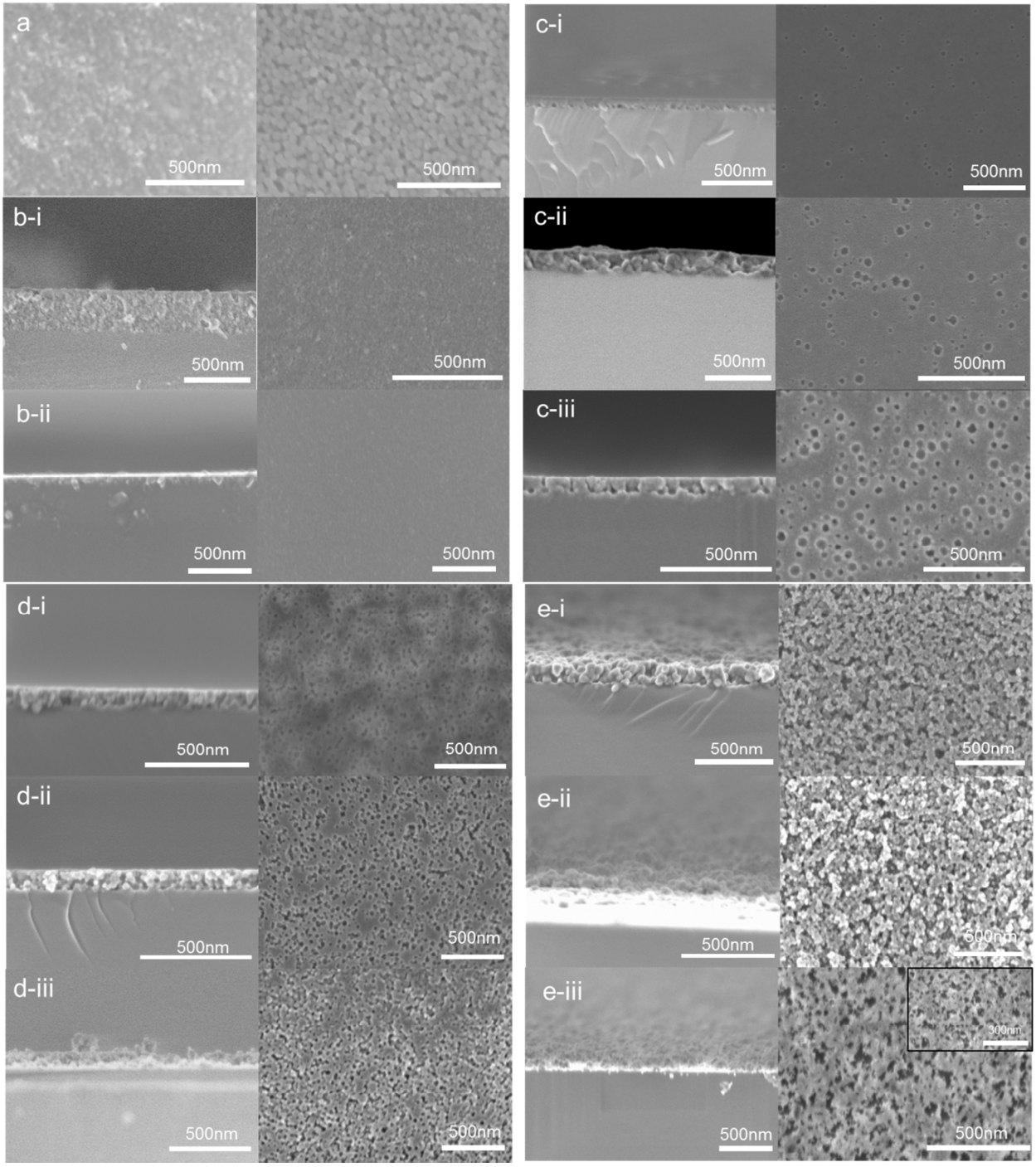

Figure 3. SEM cross-sectional and topographic images of various single layer silica films. (a) topographical view of 20nm (left) and 50nm (right) PS particle films; (b)* PS-free silica films for pre-dilutions (1:*n*) of the silica solution: b-i) 1:0; b-ii) 1:2; (c)* low PS mass ratio based silica films (pre-dilution (1:*n*), PS:SiO2 mass ratio *x*): c-i) 1:5 , 0.3; c-ii) 1:0 , 4; c-iii) 1:5 , 1.0; (d)* moderate PS mass ratio d-i) 1:3 , 2.0; d-ii) 1:1 , 6.5; d-iii) 1:0 , 10; e) high PS

mass ratio based films e-i) 1:1 , 8 e-ii) 1:3 , 10 e-iii) 1:7 , 7.0. *cross-sectional (left) and topograical (right) views.

The SEM cross-sectional and topographical images of each of the 3-layer ARC films used in the single interface and dual interface glass samples are shown in Figure 4. Each ARC clearly exhibits 3 discrete layers. The lower porosity of the intermediate layer was also exposed by deliberate partial delamination of the top layer. The transmittance spectra of a 3 layer ARC on a single glass interface, measured over a wavelength range of 400-1000nm, are shown in Figure 5-a. The spectra illustrate wavelength broadening and increasing transmittance with increasing number of tuned porous silica layers. The transmittance ranges from 94.7% to 95.4% with an average of 95.2%. The calculated transmittances, based on the following optical and physical parameters [1.32 100nm], [1.24 65nm] and [1.12 75nm], are also shown (pale lines). The calculated transmittances exhibit good agreement with the measured results, demonstrating the discrete character of the individual porous layers and their cumulative effect of rendering an ARC with optimal optical parameters.

The transmittance spectra of the two 3 layer ARCs on both interfaces of the glass substrate are shown in Figure 5-b. The measured transmittances range from 94.0% to 95.0% for the first 3 layer ARC on a single interface of glass and 97.8% to 99.5% for the double interfaced ARC glass. The average transmittance of the double interfaced ARC glass is 99.0%. The calculated transmittances are based on the following optical and physical parameters [1.33 80nm], [1.21 100nm], [1.13 100nm] for layers 1-3 on the first interface of glass, and [1.33 180nm], [1.24 120nm], [1.16 140nm] for layers 4-6 on the second interface of glass. However, the average TE and TM mode reflectance of the single interfaced ARC sample (Figure 6) at 64˚ incidence is ~25% and ~4% respectively, which may not be optimally low for large incident angles. We determined through genetic algorithm (G.A.)

an optimal angular reflectance requires a 4th layer of a slightly higher index than the 3rd layer. The 4th layer of a slightly larger index compensates for the decrease in phase thickness of the ARC layers by $n \cdot \cos(\theta)$ with increasing incident angles which in turn will increase the reflectance at normal incidence. An angular incidence optimized single interfaced ARC will have TE and TM reflectance of ~22% and 1.1% at 64˚ incident angle. An angular incidence G.A. optimized double interfaced ARC will have TE and TM reflectance of ~6.5% and 1.6% at 64˚ incident angle, which is lower than the measured values of 7.5 % and 2.5% of the double interfaced ARC sample. We summarize these results in Table 1.

Layer from the glass interface	L1	L2	L3	L4 (G.A)	L1	L2	L 3	L4 (G.A)	Average T(%) at normal incidence	Average T(%) over angular incidence
Single side ARC	1.32 100nm	1.24 65nm	1.12 75nm	--	--	--	--	--	95.2%	87.1%
Single side ARC (G.A)	1.33 124nm	1.13 144nm	1.04 196nm	1.07 44nm	--	--	--	--	95.6%	89.6%
Double side ARC	1.33 80nm	1.21 100nm	1.13 100nm	--	1.33 180nm	1.24 120nm	1.16 140nm	--	99.0%	89.4%
Double side ARC (G.A)	1.36 71nm	1.14 57nm	1.12 69nm	1.13 54nm	1.42 64nm	1.24 60nm	1.07 98nm	1.19 48nm	98.2%	92.9%

Table 1. Optical parameters of fabricated ARCs and Genetically Algorithm (G.A) optimized ARCs. (L# indicates the Layer number; optical parameters include index and thickness; averge transmittances (T) are also shown).

Using an AM1.5g solar simulator we measured the IV characteristics of a silicon cell covered with glass (denoted A), the identical cell covered with a 3 layer silica ARC glass

(denoted B) and with a double side coated 3 layer ARC glass (denoted C); the IV characteristics are shown in Figure 7. The silicon cell covered with the Corning glass and the ARC Corning glasses (single and dual side ARCs) exhibit short circuit current densities of Jsc^A = 35.1 mA/cm², Jsc^B = 36.4 mA/cm² and Jsc^C = 37.2 mA/cm², respectively; the open circuit voltages (V_{oc}) of the cells were identical at 0.53V. The single side ARC glass covered cell displays a 4.0% increase in the photogenerated current density compared to the uncoated glass covered cell. This increase matches the relative increase in transmittance of the ARC glass of 4.4%. It is noteworthy that the change in the solar spectrum weighted transmittance of the ARC glass compared to the uncoated glass is similar, indicative of the broadband enhancement. Further, the increase in the photovoltaic conversion efficiency of the cell matches the increase in the short circuit current density considering identical V_{oc}s and fill factors. For the double side ARC glass, the increase in photocurrent density is 6.0%, which is lower than the ~8% increase in optical transmittance, probably due to a greater index mismatch in the silicon-ARC interface than in the silicon-glass interface. The EQE spectrum of cell configuration B (Figure 7 inset) corroborates the broadband enhancement in transmittance for a single interface 3 layer ARC (Figure 5a) with a 3.2-4.1% increase.

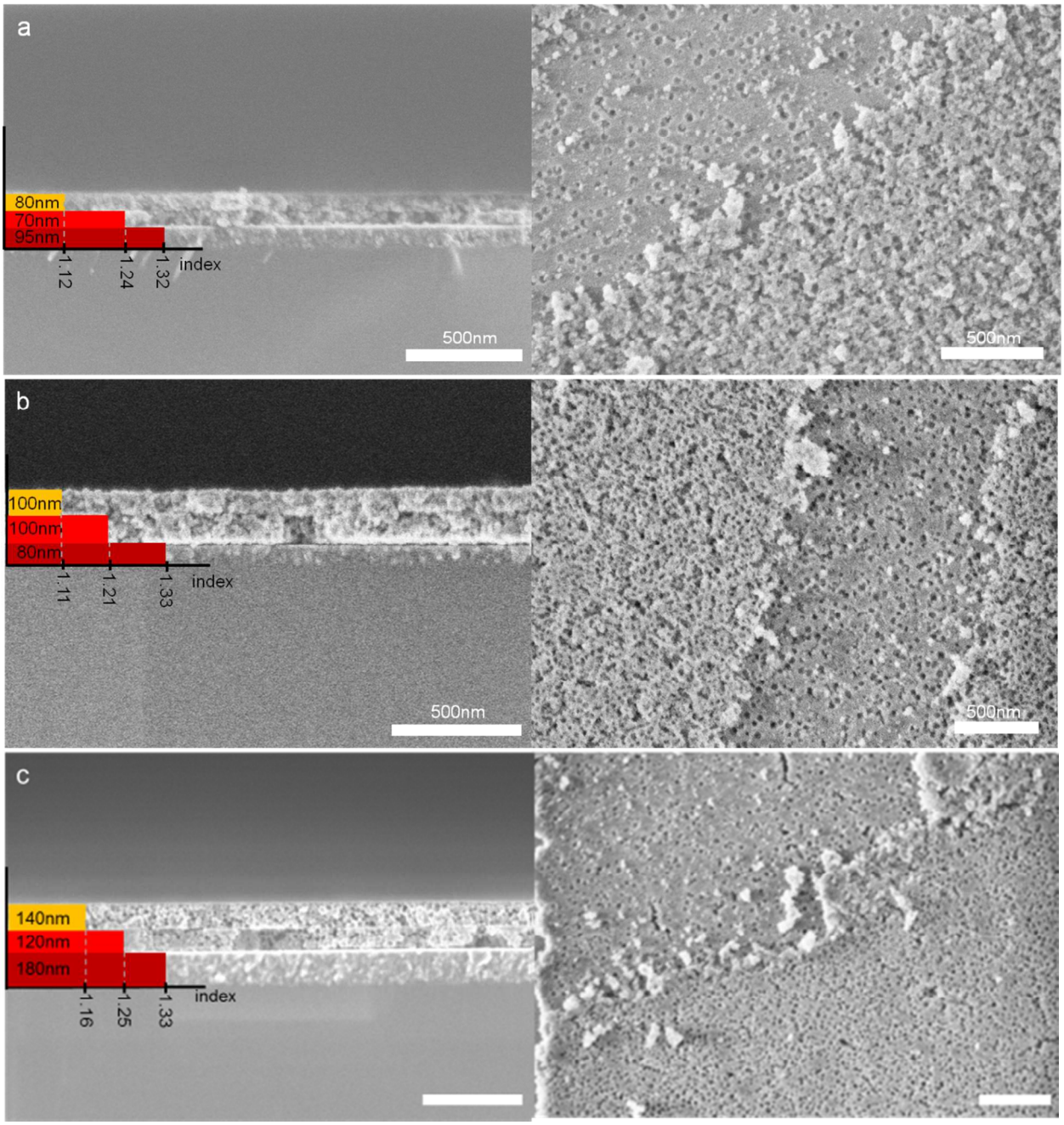

Figure 4. SEM cross sectional and topographical image of several 3 layer ARCs on a silicon substrate. Left: cross sectional view. Right: partial delamination shows the top and underlying porous layers. a): ARC optimized for one interface of the glass substrate. b) and c): ARC optimized for both interfaces of the glass substrate.

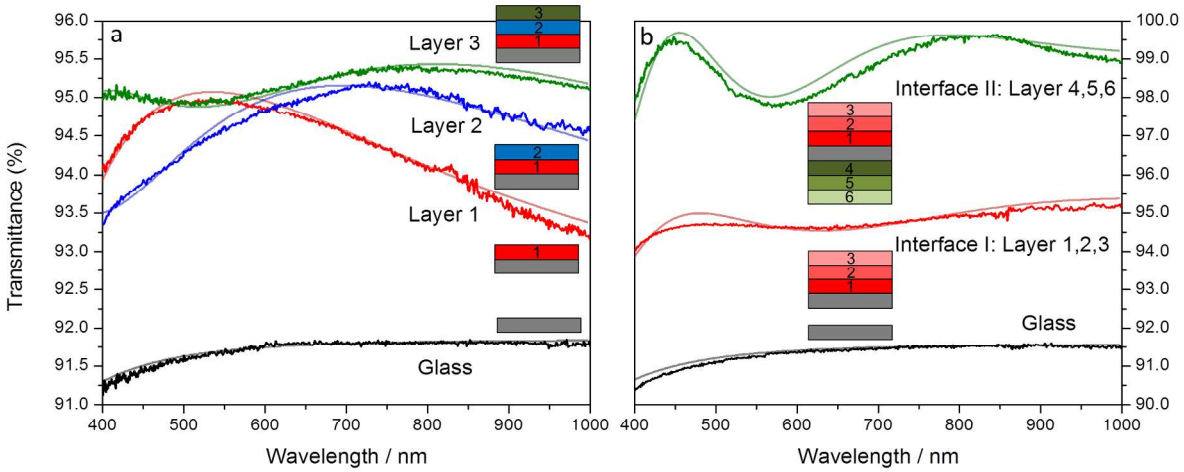

Figure 5a): Transmittance spectra of the step-wise progression of a 3 layer ARC on one glass interface. b): Transmittance spectra of two 3 layer ARCs on both interfaces of glass. Measured and calculated spectra correspond to ARCs on the first interface and the two ARCs on both interfaces. The thick and thin lines represent the measured and calculated transmittances, respectively.

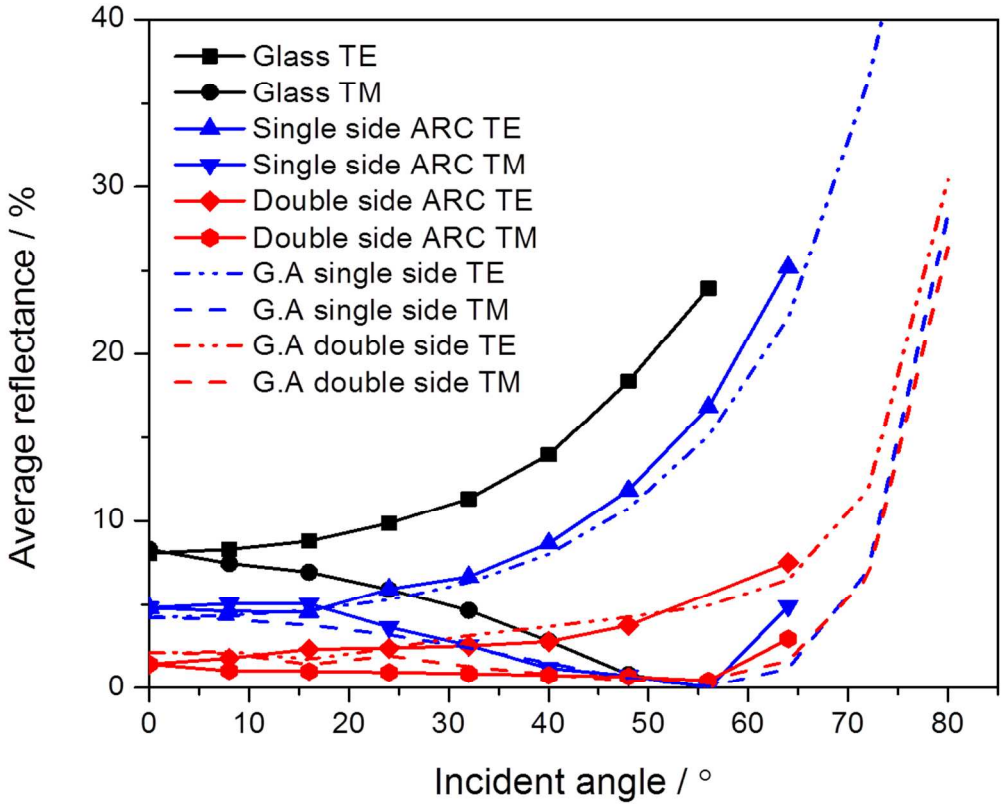

Figure 6 Measured TE and TM reflectance (spectrum averaged) of uncoated glass, 3-layered single interfaced ARC and 3-layered double interfaced ARC genetic algorithm (G.A.) optimized TE (dash-dotted lines) and TM (dashed lines) reflectance of 4-layered single interfaced ARC and 4-layered double interfaced ARC.

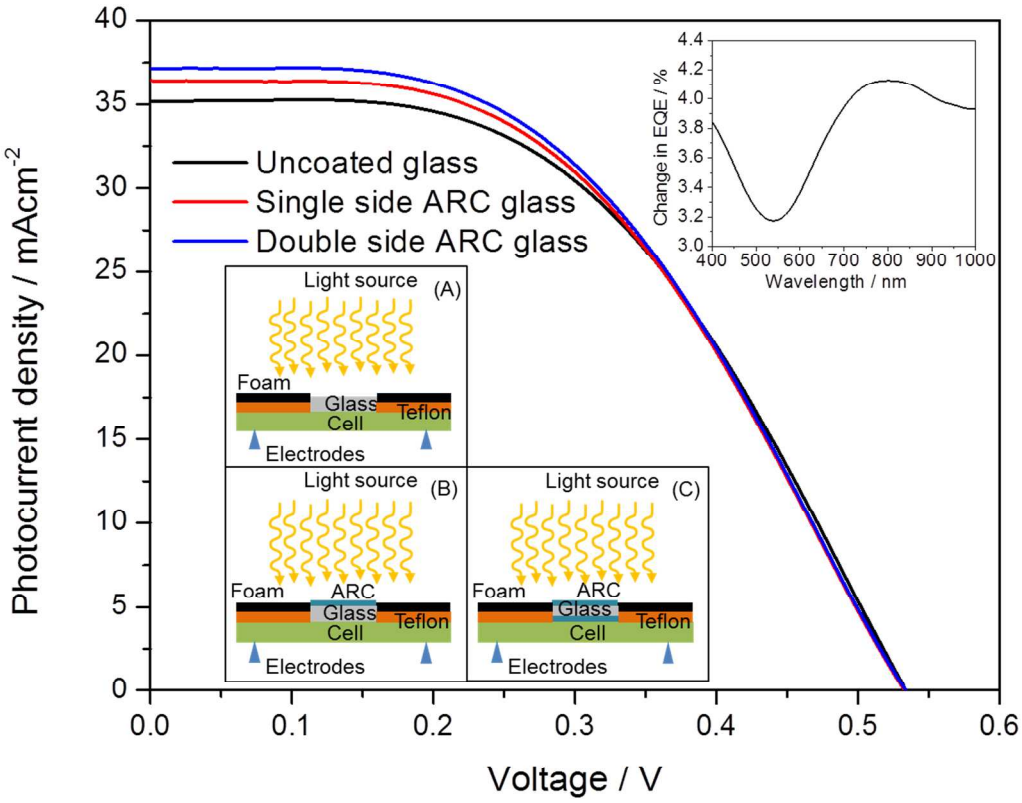

Figure 7 IV characteristics of a crystalline silicon solar cell covered with Corning glass (A), covered with a 3 layer ARC on a single glass interface (B), and for that covered with 3 layer ARCs on both sides of glass (C). Inset: EQE spectrum of the cell configuration (B) confirming the broadband enhancement in transmittance for a single interface 3 layer ARC.

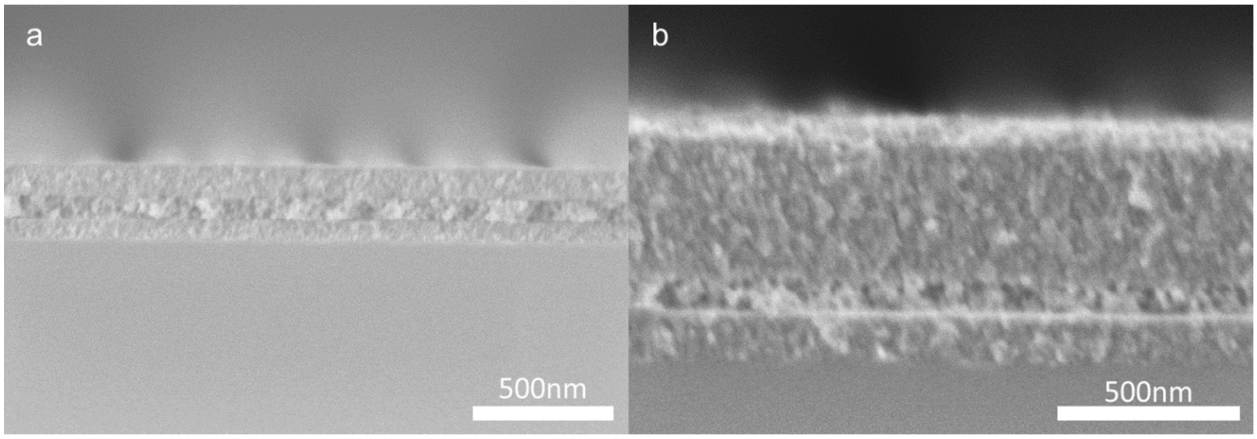

Figure 8 Examples of multilayer silica nanoparticle films wherein a high porosity nanoparticle layer is stably sandwiched between two standard (porogen-free) nanoparticle films. a): 80 nm thick high porosity layer with a 150nm thick standard top layer and 100nm thick underlying layer; b): 80 nm thick high porosity layer, as in a, but with a top layer of 600 nm thickness.

Conclusions

We have investigated the implementation of nano-length scale variation of the refractive index through the control of porosity in discrete nanoparticle layers. Specifically, we have demonstrated a facile technique whereby discrete porosity modulated silica nanoparticle layers can be deposited in sequence on a substrate. Using this method, we have shown that a single 3 layer nanoparticle ARC on glass increases the average transmittance from 91% to 95.2% while the application of two 3 layer ARCs on both glass interfaces yields an average transmittance of 99.0% and peak transmittance of 99.5%. In addition to wavelength broadening, the average transmittances at angular incidences are close to optimized values. The porosity tuned nanoparticle ARCs developed in this work exhibit transmittances comparable to vacuum-based GLAD[9] and nano-lithography[18] fabricated nano-structures. This technique offers a simple alternative to tuning of the optical index and is potentially amenable to a wide range of optoelectronic applications.

The ability to produce discrete porous multilayer films in a facile manner has wider implications beyond the fabrication of multilayer ARCs. For example, graded porous structures can be used in capacitors[36], catalytic applications, etc. Further, it is also possible to produce a highly porous layer sandwiched between two standard (porogen-free) nanoparticle layers as illustrated in Figure 8. These hollowed out nanostructures can find various applications in micro-fluidics, optical waveguiding and composite material based applications.

Supplementary Information

The silicon (100) and 2mm thick Corning glass substrates were cleaned by 5 minutes of ultra-sonication in acetone followed by 5 minutes of ultra-sonication in ethanol. The substrates were air-blown dried and then underwent ozone cleaning for 30 minutes.

The spin coating speed of 3500RPM was selected partly due to the 5000RPM speed limitation of the spin coater, and also partly as an optimization between maximizing the resultant film thickness and minimizing film surface roughness. Temperatures above 250°C were necessary to vaporize the polystyrene nanoparticles, however, a high temperature ramp rate would generate cracks and high surface roughness and hence the porogen impregnated samples were introduced into the oven at ambient temperature and heated at ramp rate of 40°C min^{-1}.

Atmospheric ellipso-porosimetry measurements[29] of selected sintered SiO_2 and SiO_2/PS nanoparticle films were also conducted. Porosity values were calculated using the Lorentz-Lorenz model equation, $\left(\frac{n_{rl}^2-1}{n_{rl}^2+2}-\frac{n_{re}^2-1}{n_{re}^2+2}\right)/\left(\frac{n_{ads}^2-1}{n_{ads}^2+2}\right)$, where n_{re} is the refractive index measured at zero humidity level when pores are empty, and n_{rl} the refractive index measured when pores are filled with water solvent. No assumption on the refractive index of the skeletal network is required to calculate the porosity volume. The distribution of a spherical pore radii r_k with respect to the relative humidity is calculated using the Kelvin formula $r_K=\frac{2\gamma V_L\cos(\theta)}{RTln(H)}$ where γ is the surface tension of the adsorptive water solvent which is 7.17×10^{-2}N/m, V_L is the molar volume of the adsorptive which is $1.8\times$

$10^{-5}m^3$/mol, θ is the water wetting angle of 57°, R the ideal gas constant, T the temperature, and H is the relative humidity.

The single interfaced 3-layer ARC was fabricated by successively spin coating colloidal solutions on a 1 inch square glass substrate. The sequence followed was: (i) a layer of PS-free pre-diluted (1:4) SiO_2 solution, (ii) a layer of 20nm PS, (iii) a layer of pre-diluted (1:3) SiO_2 solution with a PS:SiO2 mass ratio of 1, (iv) a layer of 20nm PS, (v) a layer of (1:6) SiO_2 solution with a PS:SiO_2 mass ratio of 2. The second SiO_2/PS mixture requires a higher dilution of the SiO_2 solution since the wetting of the second SiO_2/PS mixture was observably less hydrophilic on the underlying 20nm PS layer. The two 3 layer ARCs optimized for both interfaces of the glass substrate was fabricated in the following sequence: 1st interface: 1 layer of SiO2 (1:5), 1 layer of 20nm PS, 1 layer of SiO2 (1:6) + 0.5PS +100mg H2O, 1layer of 20nm PS, 1layer of SiO2 (1:5) + 1.5PS + 100mg H2O; 2nd interface: 1 layer of SiO2 (1:2), 1 layer of 20nm PS, 1 layer of SiO2 (1:2) + 1PS, 1 layer of 20nm PS, 1 layer of SiO2 (1:3) + 2 PS.

With regard to the physical stability of the nanoparticle films, we calcined the multilayer films at 450°C at the conclusion of the synthesis. During handling of the samples we observed that the ARCs remain integral so long as direct handling is avoided. However, when gripping the multilayer films directly with a pair of stainless steel tweezers we observed that part of the top, most-porous layer was exfoliated; the two underlying porous layers remained intact nevertheless.

AUTHOR INFORMATION

Corresponding Author

*E-mail: kherani@ecf.utoronto.ca

Notes

The authors declare no competing financial interests.

ACKNOWLEDGMENT

This work was supported by the Natural Sciences and Engineering Research Council (NSERC) Canada, the Ontario Research Fund – Research Excellence Program and the University of Toronto.

References

(1) J. A. Dobrowolski, D. Poitras, P. Ma, H. Vakil, and M. Acree, "Toward Perfect Antireflection Coatings: Numerical Investigation," Appl. Opt. 2002, 41, 3075-3083.

(2) Thin Film Optical Filters, 3rd ed.; H. A. Macleod; Taylor & Francis, 2001.

(3) D. J. Aiken, "High performance anti-reflection coatings for broadband multi-junction solar cells", Solar Energy Materials & Solar Cells 2000, Vol 64, 393-404.

(4) M. Victoria, C. Domínguez, I. Antón, and G. Sala, "Antireflective coatings for multijunction solar cells under wide-angle ray bundles," Opt. Express, 2012, Vol 20, 8136-8147.

(5) Thin films on glass, Schott Series on Glass and Glass Ceramics, 1st ed.; H. Bach, D. Krause; Springer, 2003.

(6) H. K. Raut, V. A. Ganesh , A.S Nair and S. Ramakrishna, Anti-reflective coatings: A critical, in-depth review Energy Environ. Sci. 2011, Vol 4, 3779-3804.

(7) S. Chattopadhyay, Y. F. Huang, Y. J. Jen, A. Ganguly, K. H. Chen, L. C. Chen, Anti-reflecting and photonic nanostructures, Materials Science and Engineering: R: Reports 2010, Vol 69, Issues 1–3, 1-35.

(8) A. Thelen: "Design of a hot mirror - contest results", Opt. Soc. Am, 1995, Technical Digest SEries, Vol 17, Issues 2-7.

(9) S. Kennedy and M. Brett, "Porous Broadband Antireflection Coating by Glancing Angle Deposition," Appl. Opt. 2002, Vol 42, 4573-4579.

(10) J. Q. Xi, M. F. Schubert, J. K. Kimm, E. F. Schubert, M. Chen, S. Y. Lin, W. Liu, J. A. Smart, "Optical thin film materials with low refractive index for broadband elimination of Fresnel reflection", Nature Photonics 2007, Vol 1, 176.

(11) J. Moghal, J. Kobler, J. Sauer, J. Best, M. Gardener, A.A.R. Watt, G. Wakefield, ACS Appl. Mater. Interfaces, 4 (2011), pp. 854–859, "High-performance, single-layer antireflective optical coatings comprising mesoporous silica nanoparticles."

(12) Jungheum Yun, Tae-Sung Bae, Jung-Dae Kwon, Sunghun Lee and Gun-Hwan Lee, Nanoscale , 2012, 4, 7221-7230, "Antireflective silica nanoparticle array directly deposited on flexible polymer substrates by chemical vapor deposition"

(13) M. Yamaguchi, H. Nakayama, K. Yamada, and H. Imai , “Ultralow refractive index coatings consisting of mesoporous silica nanoparticles”, Optics Letters 2009, Vol. 34, Issue 13, 2060-2062.

(14) X. Du and J. He, “Facile Fabrication of Hollow Mesoporous Silica Nanospheres for Superhydrophilic and Visible/Near-IR Antireflection Coatings”, Chem. Eur. J. 2011, Vol 17, 8165 – 8174.

(15) Y. Du, L. E. Luna, W. S. Tan, M. F. Rubner and R. E. Cohen, “Hollow Silica Nanoparticles in UV–Visible Antireflection Coatings for Poly(methyl methacrylate) Substrates”, ACS Nano 2010, Vol 4, 7, 4308–4316.

(16) E.K. Hussmann, Key Engineering Materials, 1998, Vol 150, 49-66.

(17) D. Chen, “Anti-reflection (AR) coatings made by sol–gel processes: A review”, Solar Energy Materials and Solar Cells 2001, Vol 68, Issues 3–4, 313-336.

(18) P. B. Clapham, M. C. Hutley, “Reduction of Lens Reflexion by the “Moth Eye” Principle”, Nature 1973, Vol 244, 281 - 282.

(19) Z. Yu, H. Gao, W. Wu, H. Ge, S.Y. Chou, “Fabrication of large area subwavelength antireflection structures on Si using trilayer resist nanoimprint lithography and liftoff”, J. Vac. Sci. Technol. B 2003, Vol 21, 2874.

(20) Y.F. Huang, S. Chattopadhyay, Y.J. Jen, C.Y. Peng, T.A. Liu, Y.K. Hsu, C.L. Pan, H.C. Lo, C.H. Hsu, Y.H. Chang, C.S. Lee, K.H. Chen, L.C. Chen, "Improved broadband and quasi-omnidirectional anti-reflection properties with biomimetic silicon nanostructures", Nat. Nanotech, 2007, Vol 2, 770.

(21) H.L. Chen, S.Y. Chuang, C.H. Lin, Y.H. Lin,"Using colloidal lithography to fabricate and optimize sub-wavelength pyramidal and honeycomb structures in solar cells", Opt. Express, 2007, Vol 15, 14793.

(22) C. Lee, S.Y. Bae, S. Mobasser, H. Manohara, "A Novel Silicon Nanotips Antireflection Surface for the Micro Sun Sensor", Nano Letters, 2005, Vol 5, 2438.

(23) M. J. Minot, “Single-layer, gradient refractive index antireflection films effective from 0.35 to 2.5 μm”, J. Opt. Soc. Am, 1976, Vol 66, 515.

(24) H. Sakata, “High-transmittance surface textures formed by plasma etching of metallophthalocyanine films”, J. Appl. Phys, 2001, Vol 89, 7711.

(25) K. Yamada, M. Umetani, T. Tamura, Y. Tanaka, H. Kasa, J. Nishii, “Antireflective structure imprinted on the surface of optical glass by SiC mold”, Applied Surface Science, 2009, Vol 255, Issue 7, 4267-4270.

(26) Y. M. Song, H. J. Choi, J. S. Yu, Y. T. Lee, “Design of highly transparent glasses with broadband antireflective subwavelength structures”, Optics express, 2010, Vol 18, 12. [25] D. J. Poxson, M. F. Schubert, F. W. Mont, E. F. Schubert, and J. K. Kim, “Broadband omnidirectional antireflection coatings optimized by genetic algorithm”, Optics Letters 2009, Vol. 34, 6. 728-730.

(27) A. Gomberta, W. Glaubittb, K. Roseb, J. Dreibholzc, B. Blaesia, A. Heinzela and D. Spornb, “Subwavelength-structured antireflective surfaces on glass”, Thin Solid Films 1999, Vol 351, 73-78.

(28) Lauri Sainiemi, Ville Jokinen , Ali Shah , Maksim Shpak , Susanna Aura , Pia Suvanto and Sami Franssila, “Non-Reflecting Silicon and Polymer Surfaces by Plasma Etching and Replication”, Adv. Mater. 2011, Vol 23, 122–126.

(29) P. C. Li and E. T. Yu, “Large area omni-directional antireflection coating on low index materials”, J. Opt. Soc. Am. B 2013, Vol 30, 10, 2584-2587.

(30) M. Schubert, F. Mont, S. Chhajed, D. Poxson, J. Kim, and E. Schubert, "Design of multilayer antireflection coatings made from co-sputtered and low-refractive-indexmaterials by genetic algorithm", Opt. Express 2008, Vol 16, 5290-5298.

(31) Electromagnetic Optimization by Genetic Algorithms, 1st ed.; Y. Rahmat-Samii, E. Michielssen; Wiley, 1999.

(32) A. Dewanjee, D. F. V. James, and M. Mojahedi, “Design of a shape-optimized metallic nanoheater”, J. Opt Soc Am A 2013, Vol. 30, 4, 671-676.

(33) Characterization of porous solids and powders surface area, pore size and density, 4th ed.; S. Lowell, J. E. Shields, M. A. Thomas, M. Thommes; Springer, 2003.

(34) Principles of Optics: Electromagnetic Theory of Propagation, Interference and Diffraction of Light, 7th ed.; M. Born, E. Wolf; Wiley, 1999.

(35) C. Katsidis and D. Siapkas, "General Transfer-Matrix Method for Optical Multilayer Systems with Coherent, Partially Coherent, and Incoherent Interference," Appl. Opt. 2002, Vol 41, 3978-3987.

(36) J. Yan, Q. Wang, T. Wei, Z.J Fan, "Recent Advances in Design and Fabrication of Electrochemical Supercapacitors with High Energy Densities", Advanced Energy Materials, 2013, (not yet in print)